Mon. Not. R. Astron. Soc. **????**, 1–?? (???) Printed 20 January 2011 (MN LATEX style file v2.2)

Relationship between eruptions of active-region filaments and associated flares and CMEs⋆

X.-L. Yan[1,2], Z.-Q. Qu [1], D.-F. Kong[3]

[1] *National Astronomical Observatories/Yunnan Astronomical Observatory, Chinese Academy of Sciences, Kunming, Yunnan 650011, P.R. China yanxl@ynao.ac.cn*

[2] *Graduate School of Chinese Academy of Sciences, Zhongguancun, Beijing, P.R. China.*

[3] *Jiaxing University, Jiaxing, Zhejiang, P.R.China.*

Accepted ????. Received ????; in original form ???

ABSTRACT

To better understand the dynamical process of active-region filament eruptions and associated flares and CMEs, we carried out a statistical study of 120 events observed by Big Bear Solar Observatory (BBSO), Transition Region and Coronal Explorer (TRACE), and the Extreme-ultraviolet Imaging Telescope (EIT) on board Solar and Heliospheric Observatory (SOHO) from 1998 to 2007. We combined filament observations with the NOAA's flare reports, Michelson Doppler Imager (MDI) magnetograms, and Large Angle and Spectrometric Coronagraph (LASCO) data, to investigate the relationship between active-region filament eruptions and other solar activities. We found that 115 out of 120 (about 96%) filament eruptions are associated with flares. 56 out of 105 (about 53%) filament eruptions are found to be associated with CMEs except for 15 events without corresponding LASCO data. We note the limitation of coronagraphs duo to geometry or sensitivity, leading to many smaller CMEs that are Earth-directed or well out of the plane of sky not being detected by near-Earth spacecraft. Excluding those without corresponding LASCO data, the CME association rate of active-region filament eruptions clearly increases with X-ray flare class from about 32% for C-class flares to 100% for X-class flares. We also found that the eruptions of active-region filaments associated with Halo CMEs are often accompanied by large flares (18 out of 20 events;

⋆ send offprint request to: Xiao-Li Yan

$\geqslant$ M1.0). About 92% events (11 out of 12) associated with X-class flare are associated with Halo CMEs. Such a result is due to that the Earth-directed CMEs detected as Halo CMEs are often the larger CMEs and many of the smaller ones are not detected because of the geometry and low intensity. The average speed of the associated CMEs of filament eruptions increases with X-ray flare size from 563.7 km/s for C-class flares to 1506.6 km/s for X-class flares. Excluding the active region located in the area more than 50 degrees from the solar center and 5 without corresponding MDI data, the β magnetic field configuration (about 47%; 36 out of 77) is more likely to form eruptive filaments than other ones and there are 33 filament eruptions associated with magnetic flux cancellation, 42 events associated with magnetic flux emergence, 2 events without variation of magnetic field. The average area of emergence regions is 855.9 square arcseconds. These findings may be instructive to not only in respect to the modeling of active-region filament eruptions but also in predicting flares and CMEs.

Key words: Sun: filaments, prominences; Sun: flares;Sun: coronal mass ejections (CMEs)

1 INTRODUCTION

Solar filaments are formed in magnetic loops that hold relatively cool (5000-8000K) and dense plasmas ($10^{10}-10^{11}cm^{-3}$) suspended in the hot (10^6K) corona above the solar surface. Filaments and prominences refer to the same physical structures on the Sun, when they are projected onto the disk (filaments) or extending above the limb (prominences). Moreover, they are observed as the magnetic flux rope having helical structure (Rust & Kumar 1994; Titov & Démoulin 1999; Amari et al. 1999; Gibson & Fan 2006; Gilbert et al. 2007).

It is widely accepted that filament eruptions, flares and Coronal Mass Ejections (CMEs) are different aspects of the same physical process (Shibata et al 1995; Forbes 2000; Priest & Forbes 2002). With the high spatial and temporal resolution observations by satellite-borne telescopes, more and more active-region filaments are able to be observed (Green et al. 2007; Chifor et al. 2007). The eruption mechanisms of filaments have been studied by many authors. For instance, it has been found that the eruptions of filaments may be caused by the kink instability (Sakurai, 1976; Ji et al. 2003; Fan 2003, 2005; Kliem et al. 2004; Rust & Labonte 2005; Williams et al. 2005; Török & Kliem 2004, 2005; Gibson 2006; Alexander et al. 2006; Liu et al. 2007; Cho et al. 2009) or the torus instability (Schrijver

et al. 2008; Aulanier et al. 2010). The occurrence of the two types of instabilities may be caused by magnetic cancellation (Chae et al. 2001; Zhang & Wang 2001; Jiang et al. 2001; Moon et al. 2004; Sterling et al. 2007; Chifor 2007), the change of the topology of loops overlying the filament (Nagashima et al. 2007), magnetic emergence (Feynman & Martin 1995; Wang et al. 1999; Romano et al. 2003), and a rapid change of magnetic connectivity in a bundle filament threads (Kim et al. 2001). Observationally, a number of phenomena are found to be associated filament eruptions which can help to discriminate between models, such as the direction of propagation of the brightenings consistent with the direction of the erupting filament (Tripathi et al. 2006), an apparent increase in the homogenization of the filament mass composition prior to filament eruptions (Kilper et al. 2009), endpoint brightening during the rapid ascent of the filaments (Wang et al. 2009), a bipolar double dimming formed near the two ends of the erupted filament (Jiang et al. 2006; Yang et al. 2008), and compact hard X-ray footpoint sources at the endpoints and a ribbon-like footpoint emission extending along the endpoints during the kink evolution of filaments (Liu & Alexander 2009).

It is also commonly accepted that the occurrence of CMEs is caused by a loss of stability or equilibrium of the coronal magnetic field (Low 1993; Forbes 2000; Lin & van Ballegooijen 2005). Jing et al. (2004) have investigated the relation between filament eruptions (most of their samples are quiescent filaments), flares and CMEs by using Big Bear Solar Observatory (BBSO) Hα full-disk images (Steinegger et al. 2000). They found that 56% of their samples were associated with CMEs except for those with no corresponding LASCO data. We note that faint, Earth-directed CMEs are less likely to be detected and this must have an influence on this figure. Gopalswamy et al. (2003) classified the prominence eruptions into two groups (transverse and radial direction events) and found that 72% of the prominence eruptions were clearly associated with CMEs by using the Nobeyama Radioheliograph. The studies of Wagner et al. (1981), Simnett & Harrison (1985), and Harrison et al. (1985, 1986) showed the evidence that the CME onset appeared to precede the flare onset for a few CME events. Through the investigation of 95 CME events from 1984 to 1986, Harrison (1990) found that active regions are the sources of, or related to the source of CMEs. In this paper, we focus on the relationship between the active-region filaments, flares and CMEs observed by BBSO, TRACE, and SOHO/EIT. Although the single active region events relative to the eruptive filament were investigated by many authors, establishing a firm quantitative

relation between them will require more statistical evidence. Moreover, we can make use of these statistics to make predictions in respect to the occurrence of flares and CMEs.

2 OBSERVATIONS AND METHOD

The data used in the paper are as follows:

1. Full-disk Hα line-center images from Big Bear Solar Observatory (BBSO), one station of global high-resolution Hα network (Steinegger et al. 2000). The image cadence is 1 minute, and the pixel size is about $1''$.

2.The Transition Region and Coronal Explorer (TRACE; Handy et al. 1999) 171Å, 195Å, 1600Å images with $0.''5$ pixel^{-1} and $1''$ spatial resolution and temporal resolution of about 1 minute.

3.Full-disk Fe XII 195 Å images from the Extreme-ultraviolet Imaging Telescope (EIT) on board Solar and Heliospheric Observatory (SOHO; Domingo et al. 1995) with a cadence of 12 minutes and a pixel size of $2.6''$ (Delaboudinière et al. 1995).

4. Full disk 96 minute line-of-sight magnetograms by Michelson Doppler Imager (MDI; Scherrer et al. 1995) on board SOHO (Domingo et al. 1995).

5. Geostationary Operational Environmental Satellite (GOES) soft X-ray light curves and NOAA's National Geophysical Data Center soft X-ray flare records ($ftp://ftp.ngdc.noaa.gov/STP/SOLAR\_DATA/SOLAR\_FLARES/$).

6. Large Angle and Spectrometric Coronagraph (LASCO; Brueckner et al. 1995) C2 on board SOHO (Domingo et al. 1995).

First, we used Full-disk Hα images from Big Bear Solar Observatory (BBSO), the movies of filaments loaded in TRACE homepage Web site ($http://trace.lmsal.com/POD/$), daily observation of TRACE, and Full-disk Fe XII 195 Å images from SOHO/EIT to detect the filament eruptions; Second, during the eruption of the filaments, we firstly identified the flares as sudden increases in intensity of Hα or EUV flare loops. Then we examined the GOES soft X-ray flux profiles, NOAA's flare records to identify the flares associated with the eruptions of filaments. Finally, we established that the equivalent position angles of the erupting filaments (see the similar discussion of Harrison & Sime 1989) are included by the spans of CMEs and the eruptive directions of filaments are consistent with that of CMEs. Besides, the CMEs appear in LASCO C2 coronagraph images within about 2 hours after the filament eruptions. If the conditions were satisfied in respect to the three points mentioned

above, we took the CME as being the association of filament eruptions. We coaligned the TRACE images and BBSO Hα images with SOHO/MDI magnetograms and EIT images so that we can determine the exact position of the filament eruptions with the active region number. Due to the projection effect, we only took into consideration magnetic configuration of active region within about 50 degrees from the solar center. Meanwhile, we determined magnetic flux emergence and cancellation from a time sequences of MDI magnetograms with a $300'' \times 300''$ FOV (for super active region, we adopted $500'' \times 500''$ FOV) obtained at least 12 hours prior to the filament eruption. We evaluated the magnetic flux emergence and cancellation from the magnetic field in the vicinity of the filament (Feynman & Martin 1995).

3 RESULTS OF FILAMENT ERUPTION ASSOCIATIONS

3.1 Distribution of samples

We found 120 active-region filament eruptions for which we obtained the complete observation of the eruption. Tables 1, 2 present a list of 120 active-region filament eruptions and summarize their relation to flares, CMEs, magnetic configuration, and the change of magnetic field. The columns contain observation time, active region number, the time and position of the filament eruption onset, associated flares and CMEs, CME speed, magnetic configuration, and magnetic flux emergence or cancellation. Some of these filaments were mentioned by Jing et al. (2004), Green et al. (2007), Williams et al. (2005), Rust & Labonte (2005), Schrijver et al. (2008), Yurchyshyn et al. (2001) and other researchers. Figure 1 shows the latitude distribution of the active-region filaments in our samples on the solar disk from 1998 to 2007. It is notable, and expected, that this figure resembles the typical butterfly diagram following the solar cycle. The distribution of active-region filaments yearly is plotted in Figure 2 and, again, this peaks with the solar cycle.

3.2 Relation between active-region filaments, flares, and CMEs

Before examining the statistical associations, we took one examples as a means of illustrating the relationship of active-region filaments to flares, CMEs. Figure 3 shows the filament eruption observed by SOHO/EIT in active region 9163 on 2000 September 12 (fig. 3a). The filament reached instability at 10:12UT. After the eruption of this filament, an M1.0 flare occurred in this region (fig. 3b). Additionally, a Halo CME was found to be associated with

the eruption of this filament (fig. 3c, d). Before the eruption of the filament, we found that the magnetic flux emergence (as is shown in the circled area) appeared in the vicinity of the eruptive filament (fig. 3e, f).

Figure 4 shows the heliographic latitude of flares and CMEs, which were associated with active-region filament eruptions. We used pluses to denote filament eruptions associated with flares. Asterisks denote the occurrence of both flares and CMEs. The triangles indicate the eruptions, which are associated with neither flares nor CMEs. The squares denote the fact that CMEs only took place respectively.

In our samples, 115 out of 120 (96%) of filament eruptions are found to be associated with flares. Jing et al. (2004) investigated 21 active-region filament and 85 quiescent filament eruptions. They found that 95% of active-region filament and 27% of quiescent filament eruptions are associated with flares. We obtained the similar results as Jing et al. (2004) on active-region filament by using more samples. Compared with their results on quiescent filaments, the active-region filaments have higher flare productivity.

Except for the 15 events without corresponding LASCO data, 56 out of 105 (about 53%) active-region filament eruptions are associated with CMEs. Jing et al. (2004) obtained 54% CME association rate on quiescent filaments. Gopalswamy et al. (2003) and Gilbert et al. (2000) found that 73% and 94% of the prominence eruptions are associated with CMEs. Their results are much higher than what we and Jing et al. (2004) obtained. Note that most of our samples as well as Jing et al.'s were taken from an area located in the solar disk. Filaments are a component of the CME eruptions. However, the weaker Earth-directed CMEs and the events well out of the plane of the sky cannot be as easily detected by the coronagraphs as events near the plane of the sky. Thus, our results must be considered in the light of observational issues (Yashiro et al. 2005).

Out of 13 events in which one filament eruption have no corresponding CME data, the eruptions of filaments associated with X-class flare are all associated with CMEs. Since we limited our sample (only 12 events), this result mentioned above need more events to confirm. Out of 43 events in which 7 filament eruptions have no corresponding CME data, 25 out of 36 (about 69%) events associated with M-class flare are associated with CMEs. Out of 52 events in which 5 filament eruptions have no corresponding CME data, 15 out of 47 (32%) events associated with C-class flare are associated with CMEs. Figure 5 shows the distribution of associated CME speed by associated flare class. The average speeds of CMEs associated with C-class, M-class, and X-class flares are 563.7, 770.3, and 1506.6 km/s

respectively. 54 out of 105 (about 51%) active-region filaments produce both flares and CMEs. Simultaneous occurrence rate of associated flares and CMEs obtained by us is higher than that obtained by Jing et al. (2004) (9 out of 19; about 47%).

3.3 The magnetic configuration of active regions with filaments

If the active region is located far away from solar disk center, the projection effect affects the judgement of magnetic configuration. Excluding the active regions located beyond 50 degrees from the solar center, the numbers of different magnetic configurations (Hale & Nicholson 1938) are shown in the figure 6. The β magnetic field configuration (about 47%; 36 out of 77) is more likely to form eruptive filaments than other magnetic configurations. Among these examples, 20 Halo CMEs are found. Excluding four active regions located in the area more than 50 degrees from the solar center, the active regions with $\beta\delta\gamma$ (7 out of 16) and β (8 out of 16) magnetic field configuration are more likely to produce Halo CMEs than other active regions.

3.4 The change of magnetic field before eruptions of filaments

For the same reason mentioned above, we excluded the active regions beyond 50 degrees from the solar center and 5 ones lacking MDI data. After the differential rotation correction, we filmed a sequence of MDI magnetograms in order to examine the change of magnetic fields. The magnetic flux emergence and cancellation appeared in the vicinity of an filament and at least 12 hours prior to the filament eruption (Jing et al. 2004). We found that there are 33 filament eruptions associated with magnetic flux cancellation, 42 events associated with magnetic flux emergence, and 2 with neither of these. The size of the emergence region of the magnetic flux is from 188 $arcsec^2$ to 1924 $arcsec^2$ (fig. 7). The average area is 855.9 $arcsec^2$.

3.5 Halo CME associations

A CME with angular width of 360 degree is defined as a Halo CME. In our samples, 20 Halo CMEs are found associated with eruptions of active-region filaments. The eruptions of active-region filaments associated with Halo CMEs are often accompanied by large flares (18 out of 20; $\geqslant$M1.0). Out of 20 events, about a half events (11 out of 20; 55%) are associated with X-class flares and 7 out of 20 events (35%) are associated with M-class flares. Out

of 13 events in which one filament eruption have no corresponding CME data, 11 out of 12 (about 92%) events associated with X-class flare are associated with Halo CMEs. The Earth-directed CMEs detected as Halo CMEs are almost certainly the larger event; smaller CMEs so far from the plane of the sky are less well detected by coronagraphs. That is to say, the smaller CMEs that are not detected by the coronagraphs may be also associated with large flares.

4 CONCLUSION AND DISCUSSION

In this paper, we focused on the statistical relationship between eruptions of active-region filaments and associated flares and CMEs. We identified 120 active-region filament eruptions observed by BBSO, TRACE, and SOHO/EIT from 1998 to 2007. The main results are summarized as follows:

(1) Of the 120 events, 96% filament eruptions are found to be associated with flares;

(2) Excluding 15 events without corresponding LASCO data, 56 out of 105 (about 53%) filament eruptions are found to be associated with CMEs;

(3) Out of 13 events in which one event has no corresponding LASCO data, the eruptions of filaments associated with X-class flare are all associated with CMEs.

(4) About 92% (11 out of 12) events associated with X-class flare are associated with Halo CMEs.

(5) Out of 43 events in which seven events have no corresponding LASCO data, 25 out of 36 (about 69%) filament eruptions associated with M-class flare are associated with CMEs.

(6) Out of 52 events in which five events have no corresponding LASCO data, 15 out of 47 (about 32%) filament eruptions associated with C-class flare are associated with CMEs.

(7) The average speed of the associated CMEs of filament eruptions increases with X-ray flare size from 563.7 km/s for C-class to 1506.6 km/s for X-class flares.

(8) 54 out of 105 (about 51%) active-region filaments produce both flares and CMEs.

(9) The eruptions of active-region filaments associated with Halo CMEs are often accompanied by large flares (18 out of 20; $\geqslant$M1.0).

(10)Except for the active region located in the area more than 50 degrees from the solar center and 5 without corresponding MDI data, we found that the β magnetic field configuration (about 47%; 36 out of 77) is more likely to form eruptive filaments than other ones and there are 33 filament eruptions associated with magnetic flux cancellation, 42 events

associated with magnetic flux emergence, 2 events without variation of magnetic field. The average area of emergence regions is 855.9 square arcseconds.

Feynman & Martin (1995) and Jing et al. (2004) reported that 42% and 54% of the eruptions of quiescent filaments are associated with CMEs respectively. Compared with our results, it can be see that the CME association rate of active-region filament eruptions is nearly the same as that of quiescent filaments. We also found that active-region filaments have higher flare production than quiescent ones by using more samples. Gopalswamy et al. (2003) and Gilbert et al. (2000) reported much higher (73% and 94%) associated CMEs productions of the prominence eruptions than what we obtained (about 53%). Note that most of our samples as well as Jing et al.'s were located in the solar disk. These results might be caused by that the slow and narrow CMEs may not be visible when CMEs originate from the disk center (Yashiro et al. 2005). Without a doubt, the typical CME is the classical three-part structure with a bright outer envelope, a dark inner void, a bright filamentary core. The filament to many researchers is a part of the CME structure. Even if one do not see the internal filamentary structure for some events, in coronagraph data one never see an erupting filament without what one would call a CME. Normally, it may be useful to talk about how many CMEs contain filaments. In this paper, we focused on how many filament eruptions are associated with CMEs. Indeed, our results are affected by the detection capability of the coronagraphs. The coronagraphs did not detect the CME due to geometry or sensitivity -i.e., weaker Earth-directed CMEs, or the events well out of the plane of the sky may not be detected by the coronagraphs.

And interestingly, we found that the eruptions of active-region filaments associated with X-class flare are all associated with CMEs except for one event without LASCO data. We need make use of forthcoming data to confirm it. This result is very useful to predict the occurrence of CME. In addition, the eruptions of active-region filaments associated with Halo CMEs are often accompanied by large flares (18 out of 20; $\geqslant$M1.0). The point that merits our particular attention is that about 92% events (11 out of 12) associated with X-class flare are associated with Halo CMEs. The coronagraphs on board near-Earth spacecraft can easily detect Halo CMEs that have large angular width. However, the many smaller CMEs can not be detected duo to the geometry and low intensity. Our result shows that the Halo CMEs are often associated with large flares and we do not rule out that the smaller CMEs that are not detected by the coronagraphs may be also associated with large flares.

The instability of the magnetic loop is a hot topic in solar physics. The total twist in a

given magnetic loop is a major factor in MHD stability. Some of sudden magnetic energy release such as flares (Hood & Priest 1979), and coronal mass ejections are probably due to the kink instability of filaments(Forbes & Isenberg 1991; Lin et al. 1998; Fisher et al. 1999; Liu et al. 2003; Leka et al. 2005; Zhou et al. 2006), the torus instability of a flux rope (Roussev et al. 2003; Kliem & T*ö*rök 2006), or the reconnection between closed field lines in the streamer belt and adjacent, open field lines (Harrison et al. 2009). In particular, the eruption of the transient sigmoid (Canfield et al. 1999; Pevtsov 2002; Low & Berger 2003) or a filament with apex rotation is a more often observed phenomenon (T*ö*rök & Kliem 2005; Green et al. 2007). Ji et al. (2003) observed a failed eruption of a filament and suggested that at least a reconnection very low in the corona (possibly above the filament) and open (opening) field above that point are required for successful eruption. While, some authors suggested that reconnection beneath the erupting footpoint may destabilise the filaments or prominences and cause the eruptions (Moon et al. 2004; Chifor et al. 2006; Nagashima et al. 2007, Sterling et al. 2007). The magnetic flux emergence and cancellation were found before the eruptions of a portion of filament eruptions in our samples. Consequently, we think that magnetic flux emergence and cancellation play an important role in triggering eruptions of active-region filaments in some events. Undoubtedly, there are other factors that trigger filament eruptions. Zhang et al. (2004) suggested that CMEs large-scale acceleration and flare particle acceleration are driven by the same physical process or by multiple processes that are physically coupled in the corona. The topics relating to the way in which the instability of twisted loops comes into being and to the conditions that can cause their eruptions deserve us to further investigation.

ACKNOWLEDGMENTS

The authors thank the referee for the careful reading of the manuscript and constructive comments that improved the original version. The authors thank the BBSO, TRACE, SOHO, NOAA and GOES consortia for their data. SOHO is a project of international cooperation between ESA and NASA. Global High Resolution Ha Network is operated by the Space Weather Research Lab, New Jersey Institute of Technology. This work is supported by the National Science Foundation of China (NSFC) under grant numbers 10903027, 10673031, 10943002 and 40636031, Yunnan Science Foundation of China under grant num-

ber 2009CD120, and the National Basic Research Program of China 973 under grant number G2006CB806301.

REFERENCES

Amari, T.; Luciani, J. F.; Mikic, Z.; Linker, J. 1999, ApJ, 518, 57

Alexander, D., Liu, R., Gilbert, H. R. 2006, ApJ, 653, 719

Aulanier, G., Török, T., Démoulin, P., DeLuca, E. E., 2010, ApJ, 708, 314

Brueckner, G. E., Howard, R. A., Koomen, M. J., Korendyke, C. M., Michels, D. J., Moses, J. D. et al. 1995, solar physics, 162, 357

Canfield R. C., Hudson H. S., McKenzie D. E., 1999, J. Geophys. Res., 26, 627

Chae, J., Wang, H., Qiu, J., Goode, P. R., Strous, L., Yun, H. S. 2001, ApJ, 560, 476

Chifor, C., Mason, H.E., Tripathi, D., Isobe, H., Asai, A. 2006, 458, 965

Chifor, C., Tripathi, D., Mason, H. E., Dennis, B. R 2007, A&A, 472, 967

Cho, K. S., Lee, J., Bong, S., Kim, Y., Joshi, B., Park, Y. 2009, ApJ, 703, 1

Domingo, V., Fleck, B., & Poland, A. I. 1995, solar physics, 162, 1

Delaboudinière, J.P., Artzner, G. E., Brunaud, J., Gabriel, A. H., Hochedez, J. F., et al. 1995, solar physics, 162, 291

Fisher, G.H., Longcope, D.W., Linton, M.G., Fan, Y., Pevtsov, A.A., 1999, Workshop on stellar dynamos ASP Conference series, eds. N*úñ*es, M., Ferriz-mas, A., Vol. 178

Forbes, T. G., Isenberg, P. A. 1991, ApJ, 373, 294

Forbes, T. G. 2000, J. Geophys. Res., 105, 23153

Fan, Y., & Gibson, S. E. 2003, ApJ, 589, 105

Fan, Y. 2005, ApJ, 630, 543

Feynman, J., & Martin, S. F. 1995, J. Geophys. Res., 100, 3355

Gopalswamy, N., Shimojo, M., Lu, W., Shibasaki, K., Howard, R.A. 2003, ApJ, 586, 562

Gibson, S. E., Fan, Y. 2006, J. Geophys. Res., 111, 12103

Gilbert, H. R., Alexander, D., Liu, R. 2007, solar physics, 245, 287

Gilbert, H. R., Holzer, T. E., Burkepile, J. T., Hundhausen, A. J. 2000, ApJ, 537, 503

Green, L.M., Kliem, B., Török, T., van Driel-Gesztelyi, L., Attrill, G.D.R. 2007, solar physics, 246, 365

Hale, G.E., & Nicholson, S.B. 1938, Magnetic Observations of Sunspots, Carnegie Institution of Washington, No. 498

Hood, A. W., & Priest, E. R. 1979, solar physics, 64, 303

Harrison, R. A., Waggett, P. W., Bentley, R. D., Phillips, K. J. H., Bruner, M., Dryer, M., Simnett, G. M. 1985, solar physics, 97, 387

Harrison, R. A. 1986, A&A, 162, 283

Harrison, R. A. & Sime, D.G. 1989, A&A, 208, 274

Harrison, R. A. 1990, solar physics, 126, 185

Harrison, R. A., Davis, C.J., Davies, J.A. 2009, solar physics, 259, 277

Handy, B. N., Acton, L. W., Kankelborg, C. C., et al. 1999, solar physics,, 187, 229

Ji, H. S., Wang, H., Schmahl, E. J., Moon, Y. J., Jiang, Y. C. 2003, ApJ, 595, 135

Jing, J., Yurchyshyn, V. B., Yang, G., Xu, Y., Wang, H., 2004, ApJ, 614, 1054

Jiang, Y.C., Li, L.P., Yang, L.H. 2006, Chinese Astron. Astrophys., 6, 345

Jiang, Y.C., & Wang, J.X. 2001, A&A, 367, 1022

Kim, Jung-Hoon, Yun, H. S., Lee, S., Chae, J., Goode, P. R., Wang, H., 2001, ApJ, 547, 85

Kliem, B., Titov, V. S., Török, T. 2004, A&A, 413, 23

Kliem, B. & Török, T. 2006, Phys. Rev. Lett., 96, 255002

Kilper, G., Gilbert, H., Alexander, D. 2009, ApJ, 704, 522

Lin, J., Forbes, T.G., Isenberg, P.A., Démoulin, P., 1998, ApJ, 504, 1006

Lin, J., & van Ballegooijen, A. A. 2005, ApJ, 629, 582

Low, B. C. & Smith, D. F. 1993, ApJ, 410, 412

Low, B. C. & Berger, M. A. 2003, ApJ, 589, 644

Leka, K.D., Fan, Y., Barnes, G. 2005, ApJ, 626, 1091

Liu, R., Alexander, D., Gilbert, H. R. 2007, ApJ, 661, 1260

Liu, R., & Alexander, D. 2009, ApJ, 697, 999

Liu, Y., Jiang, Y.C., Ji, H.S., Zhang, H.Q., Wang, H.M., 2003, ApJ, 593, 137

Moon, Y. J., Chae, J., Choe, G. S., Wang, H., Park, Y. D., Cheng, C. Z. 2004, JKAS, 37, 41

Nagashima, K., Isobe, H., Yokoyama, T., Ishii, T. T., Okamoto, T. J., Shibata, K. 2007, ApJ, 668, 533

Priest, E. R., Forbes, T. G. 2002, ARA&A, 10, 313

Pevtsov, A. A. 2002, solar physics, 207, 111

Roussev, I.I., Forbes, T.G., Gombosi, T.I., Sokolov, I.V., Dezeeuw, D.L., Birn, J. 2003, ApJ, 588, 45

Rust, D.M., Kumar, A. 1994, solar physics, 155, 69

Rust, D.M., Labonte, B.J. 2005, ApJ, 622, L69

Romano, P., Contarino, L., Zuccarello, F. 2003, solar physics, 218, 137

Steinegger, M., Denker, C., Goode, P.R., Marquette, W.H., Varsik, J., Wang H., et al. 2000, in The Solar Cycle and Terrestrial Climate, ed. A. Wilson (ESA SP-463; Noordwijk: ESA), 617

Simnett, G.M. & Harrison, R.A. 1985, solar physics, 99, 291

Sakurai, K. 1976, solar physics, 47, 261

Scherrer, P. H. et al. 1995, solar physics, 162, 169

Shibata, K., Masuda, S., Shimojo, M., Hara, H., Yokoyama, T., Tsuneta, S., Kosugi, T., Ogawara, Y. 1995, ApJ, 451, 83

Sterling, A. C., Moore, R. L., Berger, T. E., Bobra, M., Davis, J. M., et al. 2007, PASJ, 59, 823

Schrijver, C. J., Elmore, C., Kliem, B., Török, T., Title, M., 2008, ApJ, 674, 586

Titov, V.S., Démoulin, P. 1999, A&A, 351, 707

Török, T., Kliem, B., Titov, V.S. 2004, A&A, 413, 27

Török, T., Kliem, B. 2005, ApJ, 630, 97

Tripathi, D., Isobe, H., Mason, H. E. 2006, A&A, 453, 1111

Wagner, W.J., Hildner, E., House, L., Sawyer, C., et al. 1981, ApJ, 244, L123

Wang, Y. M., Sheeley, N. R. 1999, ApJ, 510, 157

Wang, Y. M., Muglach, K., Kliem, B. 2009, ApJ, 699, 133

Williams, D.R., Török, T., Démoulin, P., van Driel-Gesztelyi, L., Kliem, B., 2005, ApJ, 628, 163

Yurchyshyn, V.B., Wang, H.M., Goode, P.R., Deng, Y.Y. 2001, 563, 381

Yashiro, S., Gopalswamy, N., Akiyama, S., Michalek, G., & Howard, R. A. 2005, J. Geophys. Res., 110, 12

Yang, L.H., Jiang, Y.C., Ren, D.B. 2008, Chinese Astron. Astrophys., 8, 329

Zhou, G.P., Wang, J.X., Zhang, J., Chen, P.F., Ji, H.S., Dere, K. 2006, ApJ, 662, 35

Zhang, J. & Wang, J.X. 2001, ApJ, 554, 474

Zhang, J., Dere, K. P., Howard, R. A., Vourlidas, A. 2004, ApJ, 604, 420

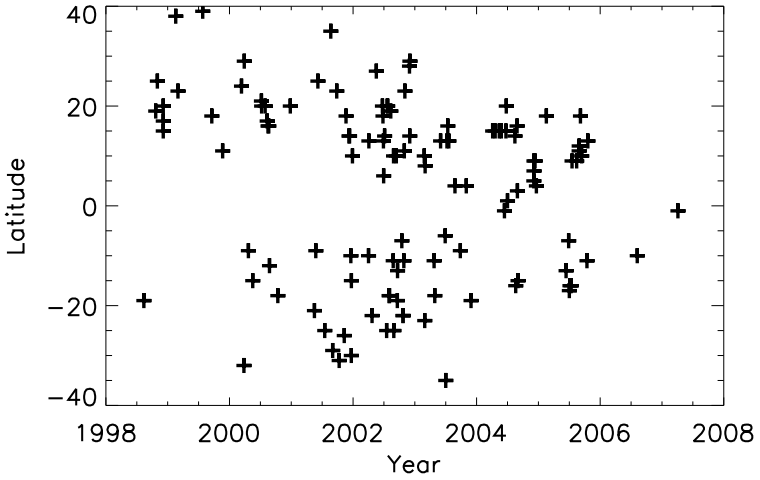

Figure 1. The distribution of active-region filaments on the solar disk from 1998 to 2007.

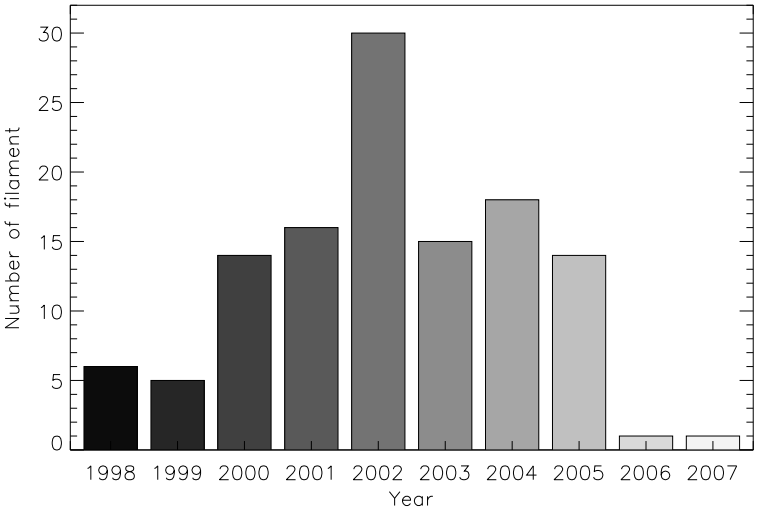

Figure 2. The distribution of active-region filaments yearly in our samples from 1998 to 2007.

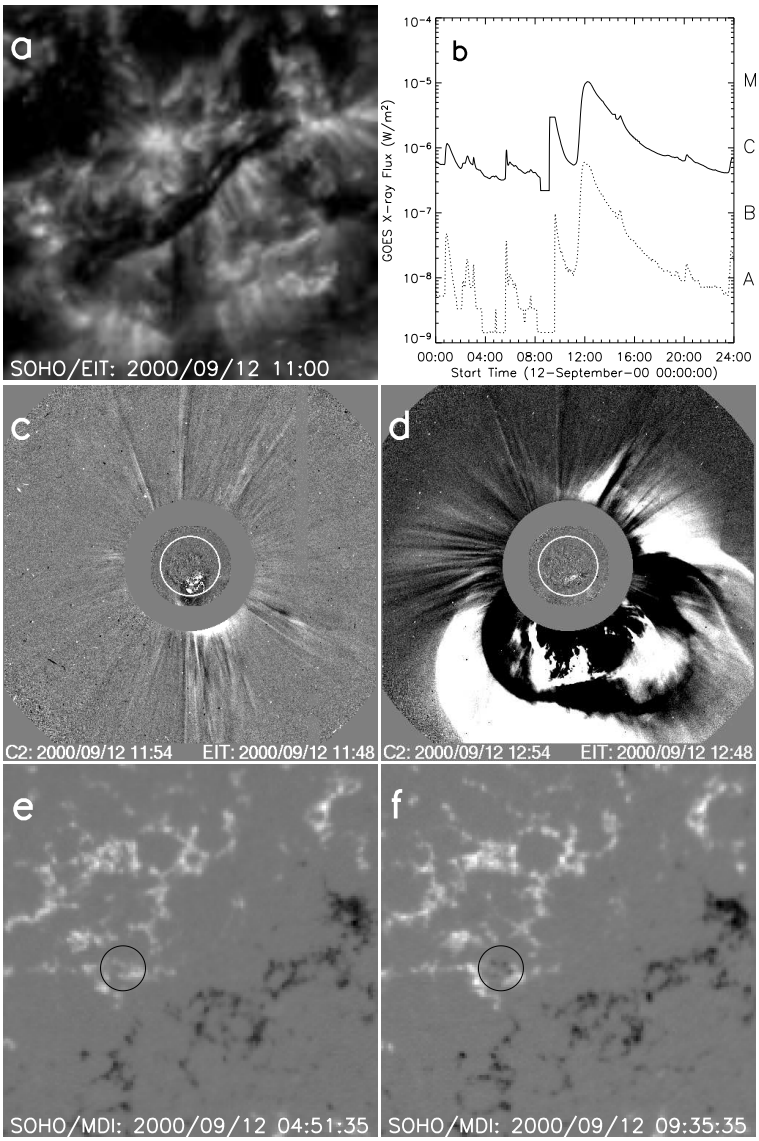

Figure 3. a: A filament in Active Region 9163 observed by SOHO/EIT. b: Evolution of GOES soft X-ray emission (Solid line: 1-8 Å; Dashed line: 0.5-4 Å) for the M6.3 flare on 2000 September 12. c and d: SOHO/LASCO running difference images of the white-light CME after eruption of the filament. e and f: The SOHO/MDI magnetograms of active region 9163. The circles indicate the position of magnetic flux emergence.

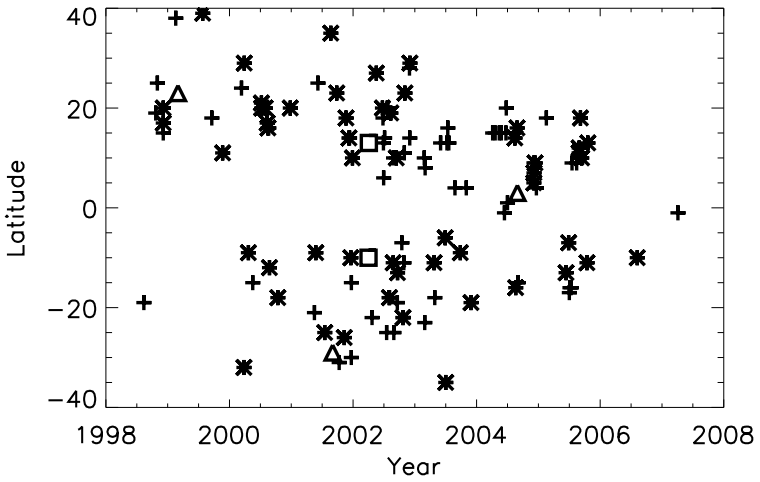

Figure 4. Latitude distribution of eruptive filaments and their overall relation to flares and CMEs. Pluses denote filament eruptions, which were associated with flares. Asterisks refer to filament eruption associated with both flares and CMEs, triangles to neither flares nor CMEs related, squares to only CMEs.

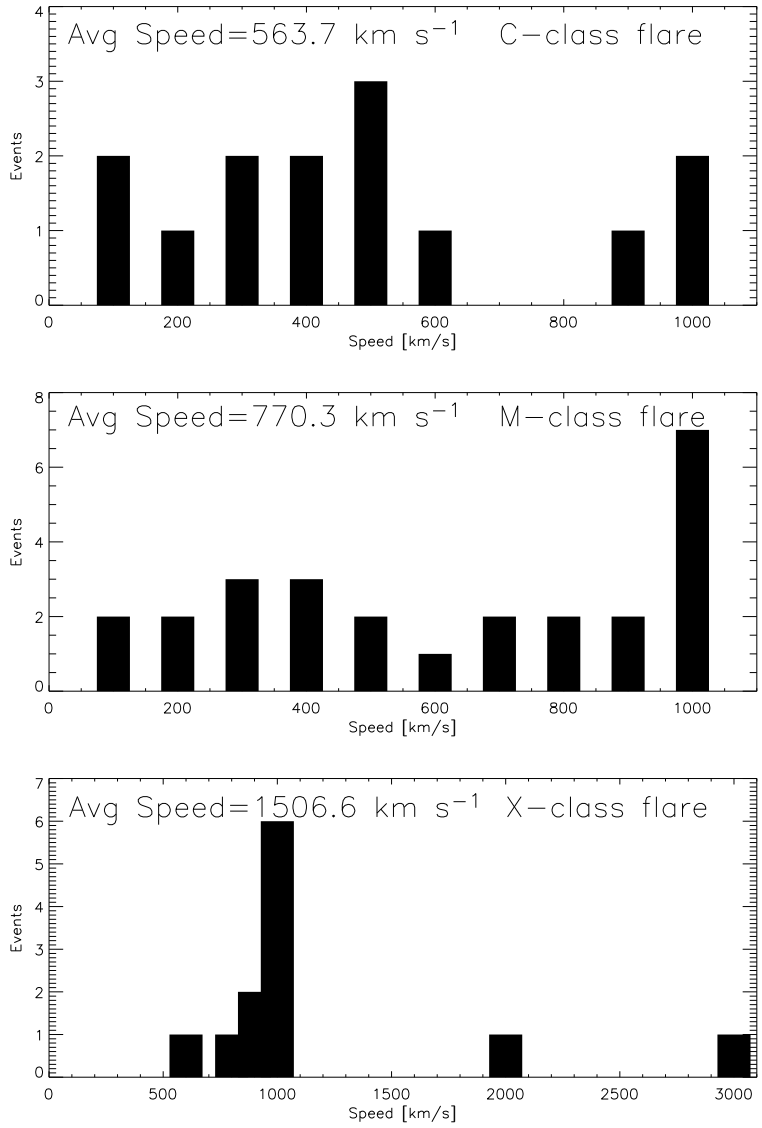

Figure 5. Distribution of associated CME speed by associated flare size respectively.

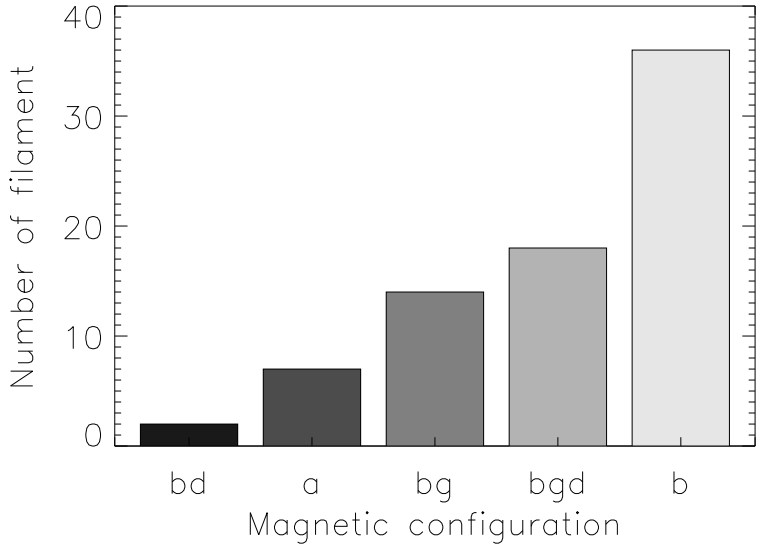

Figure 6. The numbers of active-region filaments with different magnetic configurations. "bd","a", "b", "bg", and "bgd" indicate $\beta\delta$, α, β, $\beta\gamma$, $\beta\gamma\delta$ respectively.

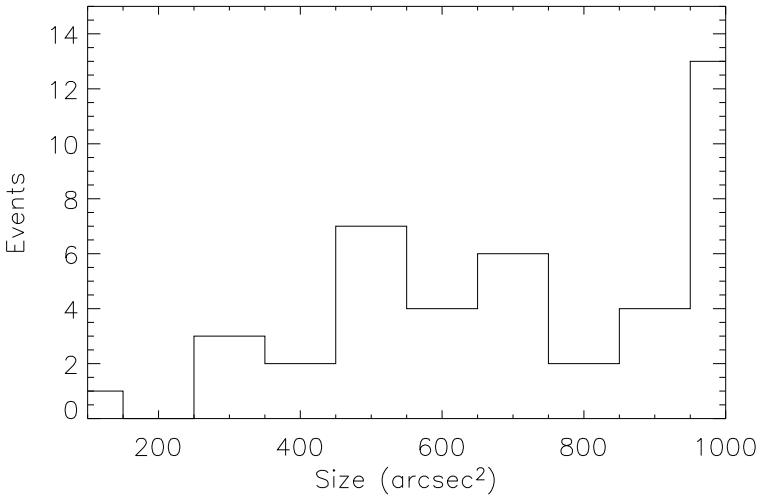

Figure 7. The numbers of events with the different sizes of the emergence regions of the magnetic flux.

TABLE 1
A list of active-region filament eruptions and their associated solar activities. "AR" indicates the active region number. "Time" and "Location" indicate the time and position of the filament eruption onset. "CME Speed" indicates linear Speed of CME. "Hale" indicates the magnetic configuration of the active region. "MFE" and "MFC" indicate the magnetic flux emergence and cancellation. "No Data" in the sixth and ninth columns denotes no LASCO observation data covering the process of the filament eruptions and no magnetograms data prior to the filament eruptions. "No" in the ninth columns denotes no obvious change of magnetic fields before filament eruption. A CME with angular width of 360 degree is defined as a Halo CME.

Date	AR	Time	Location	Flares	CMEs	CME Speed (km s^{-1})	Hale	MFE or MFC
1998 Jul 11	8260	04:21	S19W80	C1.7	No Data	···	···	···
1998 Sep 20	8340	02:30	N19E37	M1.8	No Data	···	···	No data
1998 Sep 30	8340	11:54	N25W90	M2.8	No Data	···	···	···
1998 Nov 4	8375	03:14	N17E01	C5.2	CME	102	$\beta\gamma$	MFE
1998 Nov 4	8375	07:13	N20E01	C1.6	Halo	523	$\beta\gamma$	MFC
1998 Nov 4	8375	22:02	N15W17	C2.4	···	···	$\beta\gamma$	MFE
1999 Jan 17	8440	17:32	N38E16	C2.5	No data	···	···	No data
1999 May 31	8559	22:06	N23W19	···	···	···	β	MFC
1999 Jun 24	8595	12:48	N39W08	C4.1	Halo	974.9	β	MFC
1999 Aug 17	8668	09:18	N18E32	C2.6	···	···	β	MFE
1999 Oct 20	8731	05:51	N11W46	M1.7	CME	326.5	$\beta\gamma$	MFC
2000 Feb 10	8858	01:04	N24E01	C7.3	···	···	β	MFC
2000 Feb 17	8872	20:04	S32E07	M1.3	Halo	727.7	β	MFC
2000 Feb 26	8889	21:47	N29E53	M1.0	CME	667.7	···	···
2000 Mar 20	8921	08:12	S09E90	M2.2	CME	1225.7	···	···
2000 Apr 16	8948	03:51	S15W80	C4.2	···	···	···	···
2000 Jun 6	9026	13:30	N24E18	M7.1	CME	357.7	$\beta\gamma\delta$	MFC
2000 Jun 7	9026	15:30	N21E02	X1.2	Halo	842	$\beta\gamma\delta$	MFC
2000 Jun 28	9051	18:31	N20W90	C3.7	CME	1198	···	···
2000 Jul 10	9070	19:40	N17W40	M1.9	CME	425.8	$\beta\gamma$	MFC
2000 Jul 14	9077	09:30	N16E01	X5.7	Halo	1674.2	$\beta\gamma\delta$	MFC
2000 Jul 19	9077	14:08	N16W70	C3.4	No data	···	···	···
2000 Jul 23	9091	04:24	S12W06	Optical	CME	630.8	α	MFE
2000 Sep 12	9163	11:03	S18W10	M1.0	Halo	1550.1	β	MFE
2000 Nov 24	9236	17:20	N20W01	X1.8	Halo	1005.5	β	MFE
2001 Apr 23	9431	12:03	S09W28	C2.8	CME	529.7	β	MFE
2001 Apr 15	9415	21:58	S21W80	C5.1	···	···	···	···
2001 May 5	9445	18:01	N25W11	C6.3	···	···	$\beta\gamma$	MFE
2001 Jun 15	9502	09:58	S25E39	M6.3	CME	1090.4	β	MFC
2001 Jul 20	9538	03:36	N35W27	B7.6	CME	193.4	α	MFE
2001 Aug 1	9557	20:28	S29W14	···	No data	···	β	MFC
2001 Aug 25	9591	16:32	S23E45	X5.3	Halo	1432.8	$\beta\gamma\delta$	MFE
2001 Sep 9	9608	20:38	S31E29	M9.5	···	···	$\beta\gamma$	MFE
2001 Oct 9	9653	10:48	S26E03	M1.4	Halo	973	β	No
2001 Oct 19	9661	16:15	N18W40	X1.6	Halo	901	$\beta\gamma\delta$	MFE
2001 Oct 28	9682	16:43	N15E29	M1.4	CME	279.4	$\beta\gamma\delta$	MFE
2001 Nov 1	9682	11:32	N14W30	M3.3	···	···	$\beta\gamma\delta$	MFC
2001 Nov 8	9690	15:45	S30E23	M4.2	No data	···	$\beta\gamma$	MFE
2001 Nov 9	9687	18:20	S15W43	M1.9	No data	···	$\beta\gamma\delta$	MFC
2001 Nov 17	9704	04:04	S10E47	M2.8	Halo	1379	β	MFE
2001 Dec 1	9724	17:39	N10E80	M1.8	CME	736	···	···
2002 Mar 2	9856	13:25	S10E90	···	CME	1131.2	···	···
2002 Mar 21	9871	18:05	S22W29	C1.3	···	···	β	MFC
2002 Apr 9	9885	07:15	N13W90	···	CME	260.3	···	···
2002 Apr 16	9893	12:53	N27W80	M2.5	CME	166	···	···
2002 May 21	9960	20:16	N20E40	M1.5	CME	853.3	β	MFE
2002 May 24	9962	20:26	N18E14	Optical	···	···	β	MFC
2002 May 27	9957	18:00	N13W75	M2.0	···	···	···	···
2002 May 28	9957	16:19	N06W90	C3.6	···	···	···	···
2002 Jun 4	9974	17:47	N14W23	C1.0	No data	···	α	MFE
2002 Jun 16	9991	21:13	S25W45	C1.2	···	···	β	MFE
2002 Jun 17	10001	22:53	N20E40	Optical	···	···	β	MFC
2002 Jun 19	10000	20:05	N20W15	Optical	···	···	β	MFE
2002 Jul 1	10016	20:32	S18W09	C1.0	···	···	β	MFE
2002 Jul 4	10019	16:09	S18E06	C3.4	CME	343.1	$\beta\gamma$	MFE
2002 Jul 15	10030	20:04	N19E01	X3.0	Halo	1151	$\beta\gamma\delta$	MFC
2002 Jul 23	10039	00:16	S11E65	X4.8	Halo	2285	···	···
2002 Jul 26	10046	15:37	N10W24	Optical	···	···	α	MFE

TABLE 2
Continue

Date	AR	Time	Location	Flares	CMEs	CME Speed (km s^{-1})	Hale	MFE or MFC
2002 Aug 14	10067	19:34	N10E17	M1.4	CME	323.6	β	MFE
2002 Aug 18	10083	16:41	S19E52	C6.0	···	···	···	···
2002 Aug 19	10069	20:56	S13E33	M3.1	CME	804.9	$\beta\gamma\delta$	MFE
2002 Sep 14	10105	17:07	S07W08	C4.5	···	···	$\beta\gamma\delta$	MFC
2002 Sep 18	10119	23:04	S22E03	C1.0	···	···	β	MFE
2002 Sep 21	10119	16:50	S15W33	C2.6	CME	431.4	$\beta\gamma\delta$	MFE
2002 Sep 21	10123	20:11	S11W22	C2.6	···	···	β	MFE
2002 Sep 29	10134	06:33	N11E17	M2.6	···	···	$\beta\gamma\delta$	MFC
2002 Oct 24	10162	18:04	N23W15	C7.4	CME	311.7	$\beta\gamma\delta$	MFE
2002 Oct 29	10162	02:52	N28W55	M1.1	···	···	···	···
2002 Oct 31	10162	17:24	N29W90	C8.0	CME	160.5	···	···
2002 Nov 5	10177	20:51	N14W11	C3.4	···	···	$\beta\gamma$	MFC
2003 Jan 25	10268	18:32	N10W29	C4.4	···	···	$\beta\delta$	MFC
2003 Jan 29	10266	20:13	S23W61	C1.1	···	···	···	···
2003 Mar 26	10321	16:57	N08E59	C2.2	···	···	···	···
2003 Mar 29	10318	18:27	S11W21	C8.2	CME	633.8	β	MFC
2003 May 2	10345	02:25	S18W25	M1.0	···	···	β	MFC
2003 May 27	10365	22:48	S06W14	X1.3	Halo	964.5	β	MFE
2003 May 29	10368	17:29	S35W14	M2.8	CME	266.2	β	MFC
2003 Jun 2	10375	17:25	N13E70	M1.8	···	···	···	···
2003 Jun 11	10375	20:20	N13W59	X1.6	No data	···	···	···
2003 Jun 12	10375	01:06	N16W55	M7.3	No data	···	···	···
2003 Jun 12	10375	17:15	N13W81	M1.1	No data	···	···	···
2003 Aug 25	10442	01:34	S09E38	C3.6	CME	574.8	β	MFC
2003 Sep 29	10464	19:45	N04W41	C3.8	···	···	$\beta\gamma$	MFC
2003 Oct 24	10484	21:33	N04W05	M1.0	···	···	$\beta\gamma\delta$	MFC
2003 Dec 2	10508	09:24	S19W90	C7.2	CME	1392.7	···	···
2004 Mar 24	10582	18:38	N15E90	C1.5	···	···	···	···
2004 Mar 24	10582	20:14	N15E90	C7.4	···	···	···	···
2004 Mar 24	10582	23:20	N15E90	M1.5	···	···	···	···
2004 Mar 29	10582	18:27	N15E16	C3.4	···	···	···	No data
2004 Mar 30	10581	22:46	S01E04	C2.0	No data	···	α	No
2004 May 12	10609	15:34	N01E41	C1.3	···	···	β	MFE
2004 May 21	10615	22:10	N15E02	C1.2	···	···	α	MFE
2004 May 24	10615	22:32	N20W35	C1.0	···	···	β	MFE
2004 Jul 13	10646	00:00	N14W41	M6.7	CME	408.9	β	MFE
2004 Jul 26	10652	16:52	N16W50	M1.1	CME	400.9	···	No data
2004 Jul 26	10652	17:31	N03W45	···	···	···	···	No data
2004 Aug 12	10656	15:58	S15W05	C6.5	···	···	$\beta\gamma\delta$	MFE
2004 Aug 18	10656	17:37	S16W90	X1.8	CME	601.5	···	···
2004 Nov 3	10696	17:54	N05E23	M1.0	CME	513.2	β	MFC
2004 Nov 4	10696	21:32	N07E12	M2.5	CME	1054.5	$\beta\gamma$	MFC
2004 Nov 4	10696	22:41	N09E09	M5.4	···	···	$\beta\gamma$	MFC
2004 Nov 10	10696	02:01	N09W50	X2.5	Halo	3387.1	$\beta\gamma\delta$	MFE
2004 Nov 18	10700	19:48	N04W90	C1.9	···	···	···	···
2005 Jan 16	10720	07:11	N18W10	C4.4	···	···	$\beta\delta$	MFE
2005 May 11	10758	19:19	S13W52	M1.1	Halo	550.3	···	···
2005 May 26	10767	20:59	S07E12	C8.6	CME	419.9	$\beta\gamma$	MFE
2005 Jun 1	10772	17:32	S17E41	C3.1	···	···	β	MFE
2005 Jun 1	10772	21:56	S16E39	C7.2	···	···	β	MFE
2005 Jun 6	10772	18:19	S16W22	C1.2	···	···	β	MFE
2005 Jun 16	10775	19:54	N09W90	M4.0	No data	···	···	···
2005 Jul 13	10786	19:04	N09W85	M1.2	···	···	···	···
2005 Jul 27	10792	04:40	N11E90	M3.7	Halo	1787.5	···	···
2005 Jul 28	10792	21:54	N12E90	M4.8	CME	1478.4	···	···
2005 Jul 29	10792	17:39	N18E71	C3.4	CME	296.7	···	···
2005 Jul 30	10792	05:03	N10E76	C9.4	CME	No data	···	···
2005 Jul 30	10792	05:42	N13E70	X1.3	Halo	1968.4	···	···
2005 Sep 13	10808	18:00	S11E11	X1.5	Halo	1866.1	$\beta\gamma\delta$	MFE
2006 Jul 6	10898	08:06	S10W38	M2.5	Halo	910.6	β	MFC
2007 Mar 2	10944	04:47	S01W17	B2.5	No data	···	α	MFC